

Design and characterization of orthotropic re-entrant auxetic structures made via EBM using Ti6Al4V and pure copper

L. Yang*, O. Harrysson*, H. West II* and D. Cormier†

*Edward P. Fitts Department of Industrial and Systems Engineering, North Carolina State University, Raleigh, NC 27606

†Department of Industrial and Systems Engineering, Rochester Institute of Technology, Rochester, NY 14623

REVIEWED, August 17 2011

Abstract

An orthotropic 3D re-entrant honeycomb structure that exhibits a negative Poisson's ratio was designed and fabricated via the electron beam melting (EBM) process. The modeling work established the relationships between various structural parameters and the mechanical properties of the auxetic structures. Compressive tests were performed on the re-entrant honeycomb samples made with Ti6Al4V as well as pure copper. Results of the strength, modulus and energy absorption for the two materials were compared with the theoretical models in order to verify the theoretical predictions.

Keywords: Electron Beam Melting, Auxetic Structures, Ti6Al4V, copper

Introduction

Auxetic structures have shown promise for various engineering applications such as sandwich panel cores, impact absorption, biomedical implants and aerospace structures. These structures exhibit high shear modulus [1-3], high indentation resistance, high fracture toughness [4-6], high energy absorption ability [7-10], and novel acoustic and electromagnetic absorption abilities [12-14]. The prevailing manufacturing process for synthesis of polymer auxetic structures has somewhat limited control over the mechanical properties [1, 15]. As a result, much of the modeling work involving auxetic structures has lacked experimental validation, and very limited design for specific properties has been achieved.

In this current work, the uniaxial compressive properties of a 3D re-entrant lattice structure were modeled. Compressive Ti6Al4V and pure copper samples were manufactured via the electron beam melting (EBM) process and were then evaluated via mechanical testing. The results support the validity of the analytical models, and the difference in behavior between the Ti6Al4V and the pure copper are also discussed.

Modeling Of The Structure

Fig. 1a shows a 2D re-entrant lattice structure which can be readily extended into a 3D structure as shown in Fig. 1b. The design parameters for the structures are shown in Fig. 1c, which include the length of the vertical (H) and re-entrant strut (L), the re-entrant angle (θ), and the thickness of the strut. Fig. 1b shows a simple pattern where the struts have rectangular cross sections. In practice, the shape of the cross section may vary.

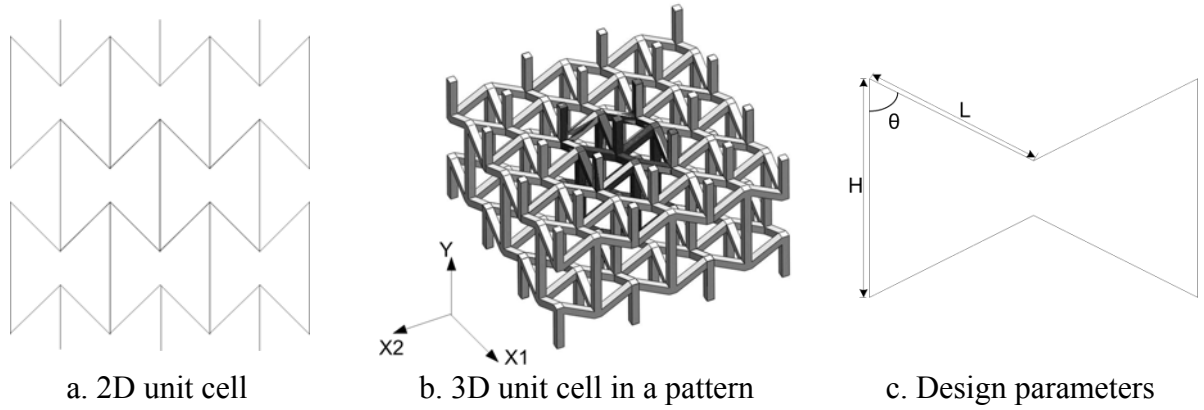


Fig. 1 Re-entrant lattice structure

From Fig. 1b it can be seen that the 3D re-entrant lattice structure is orthotropic, with two geometrically identical directions (x_1 and x_2) and a third direction (y) which is different than the other two. The auxetic behavior can be tailored to a greater extent in the y -direction due to the anisotropy of the structure. The current work therefore focuses on mechanical properties in the y -direction.

Consider a remote compressive stress (σ) applied in the y -axis direction on an infinite 3D re-entrant lattice structure. Due to the structure's symmetry, the relationship between the stress and the resulting force on the struts is simplified into the case shown in Fig. 2a, where the force components can be shown to be:

$$F = \frac{1}{2} \sigma (2L \sin \theta)^2 = 2\sigma L^2 \sin^2 \theta \quad (1)$$

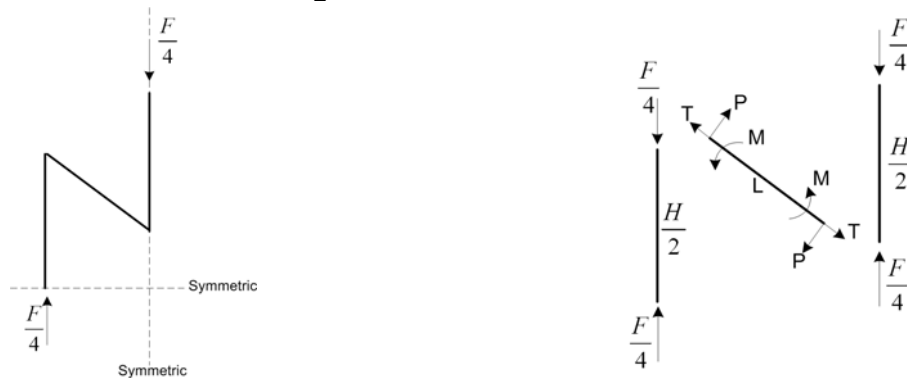


Fig. 2 Analysis of the structure under compressive loading in y -axis direction

From Fig. 2(b), the deformation of the structure is influenced by the bending of the re-entrant (e.g. diagonal) struts as well as axial compression of the vertical struts. Under the small deflection assumption [16], it is determined that the re-entrant strut is subject to critical loading. For the simple case involving struts a square cross section of thickness t , the Poisson's ratio (ν_y), the structural modulus (E_y) and the yield strength (σ_y) of the lattice can be obtained using standard beam theory as follows:

$$\nu_y = -\frac{L^2 \cos \theta (\alpha - \cos \theta)}{2\alpha t^2 + L^2 \sin^2 \theta} \quad (2)$$

$$E_y = \frac{\sigma}{\varepsilon_y} = \frac{2(\alpha - \cos \theta)}{4\alpha t^2 + L^2 \sin^2 \theta} \left(\frac{t^2}{L \sin \theta} \right)^2 E \quad (3)$$

$$\frac{(\sigma_y^2 - \frac{9F^2 \sin^2 \theta}{64t^4})t^3}{4\sigma_y} - \frac{F^2 \cos^2 \theta \sigma_y}{(64\sigma_y^2 - \frac{9F^2 \sin^2 \theta}{t^4})t} = \frac{FL}{8} \sin \theta \quad (4)$$

where $\alpha=H/L$, and E and σ are the modulus and yield strength of the bulk material, respectively. Eq. (4) is an implicit equation and can be solved numerically. Eq. (4) indicates the critical compressive force for yielding, which can be converted into the yield strength as follows:

$$\sigma = \frac{F_m}{2L^2 \sin^2 \theta} \quad (5)$$

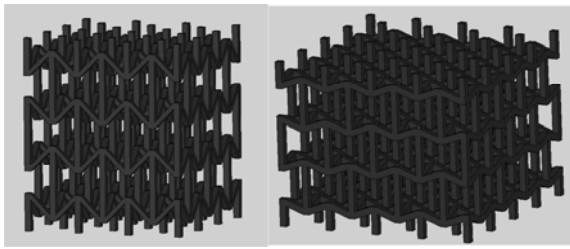
Sample design and preparation

Two different configurations were designed using the structural parameters shown in Table.1. The cross section of the struts were made square in the CAD model with different sizes for the vertical and re-entrant struts $t1$ and $t2$ respectively. The relative density (RD) was taken to be the mass of the lattice structure divided by the mass of solid block having the same bounding box dimensions. The theoretical Poisson's Ratio (PR) values were calculated by Eq. (2). As indicated in Table 1, design configuration D2 should exhibit more significant auxetic behavior due to its more negative PR value.

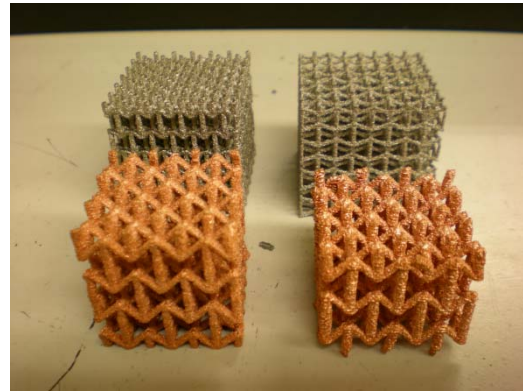
Table 1 Design parameters for experimental samples

Design	H (mm)	L (mm)	t1 (mm)	t2 (mm)	θ (°)	RD	PR
D1	7.6	4	1	0.94	70	0.1160	-0.463
D2	12	6	1	0.71	45	0.0915	-1.496

Six samples for each design configuration were produced via the electron beam melting (EBM) process using both Ti6Al4V and pure copper. Ti6Al4V samples were produced in an Arcam A-2 machine using -100/+325 mesh spherical Ti6Al4V plasma rotating electrode (PREP) powder. The copper samples were produced in an Arcam S-12 machine using -100 mesh gas atomized copper powder. In this study, the density (ρ), yield strength (S) and modulus (E) values for the solid Ti6Al4V and copper are taken as: $\rho_{Ti6Al4V}=4.43g/cm^3$, $S_{Ti6Al4V}=1050MPa$, $E_{Ti6Al4V}=114GPa$, $\rho_{Cu}=8.94g/cm^3$, $S_{Cu}=330MPa$, $E_{Cu}=119GPa$.



a. CAD models



b. Samples produced by EBM

Fig.3 Design and manufacturing of samples

After parts were produced by the EBM process, the lattice block dimensions were measured using calipers, and the strut size was measured via optical microscopy. Sample weights were recorded using a digital scale. The recorded dimensions and weights with sample standard deviations are shown in Table 2. Two strut thickness values are provided for both Ti6Al4V and copper samples, indicating that the fabricated struts had rectangular rather than square cross sections. The dimensional variation for the strut size is more significant for copper than for Ti6Al4V. It is hypothesized that this was due to the greater degree of particle sintering at the part surface introduced by high thermal conductivity. This also leads to an increased relative density of the structure, which according to the theory of cellular solids, playing a significant role in the mechanical performance of the structures [17].

The manufacturing quality of EBM for the Ti6Al4V parts is relatively consistent. However, due to the heat dissipation, some of the particles around the melted struts become lightly sintered to the struts. The surface quality of the EBM fabricated struts is therefore rather rough. Fig. 4 illustrates the deviation of strut size/form from the ideal CAD model representation introduced by the surface texture. In order to evaluate the mechanical properties, the minimum strut dimension d was adopted as the thickness values of the struts. Furthermore, the cross section of the actual struts is apparently not an idealized square and is therefore another source of deviation between the experiments and the theoretical predictions.

The process theme of the EBM process with pure copper has recently been developed in house with the implementation of the new multi-beam control, therefore copper was also used for this current study. It is worth noting that the process parameters has not been optimized for mesh structures. Due to its high thermal conductivity, it was expected that the dimensions of the copper samples would exhibit relatively large variation.

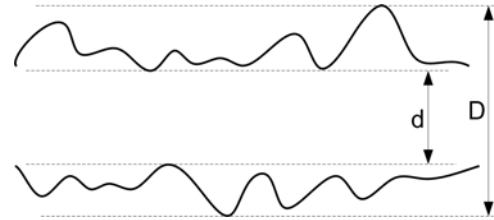
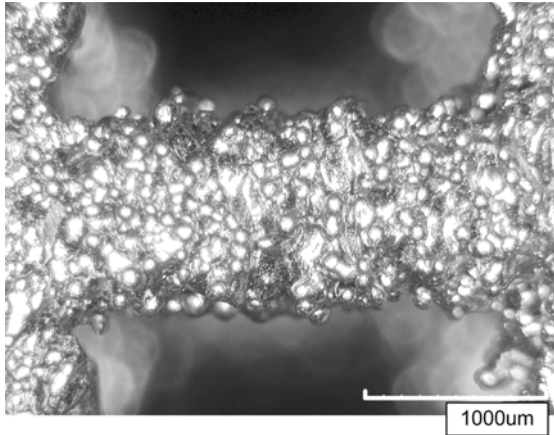


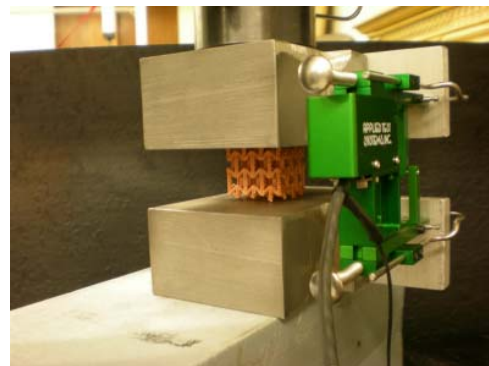
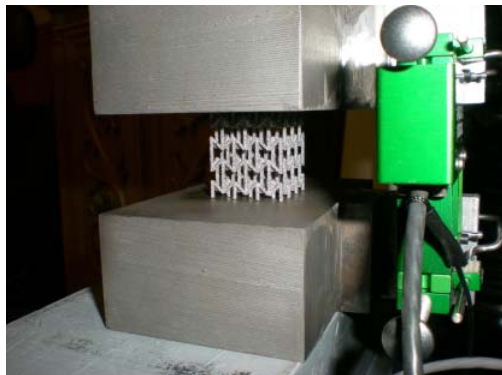
Fig. 4 Surface of EBM struts

Table 2 Unit cell dimensions of the actual parts made by EBM

Design	H (mm)	L (mm)	$t1$ (mm)	$t2$ (mm)	θ (°)	RD
Ti6Al4V						
D1	7.436 ± 0.031	4.101 ± 0.008	1.085 ± 0.044	1.180 ± 0.028 (1.078 ± 0.076)	70	0.142 ± 0.005
D2	11.945 ± 0.016	6.238 ± 0.005	1.076 ± 0.045	1.155 ± 0.034 (0.815 ± 0.020)	45	0.115 ± 0.002
Copper						
D1	7.255 ± 0.170	4.197 ± 0.026	1.209 ± 0.146 (1.698 ± 0.059)	1.973 ± 0.214 (1.106 ± 0.150)	70	0.208 ± 0.005
D2	12.526 ± 0.118	6.375 ± 0.043	1.507 ± 0.087 (1.160 ± 0.101)	1.517 ± 0.181 (1.045 ± 0.115)	45	0.155 ± 0.002

Experiments and results

Compression tests were performed on an Applied Test Systems 1620C Universal Testing Machine, with maximum loading of 89000N. Two case hardened steel platens were used to perform the compressive tests. An extensometer was attached directly to the platens, as they cannot be attached to the lattice block samples. Fig. 5 shows the layout of the experiments.



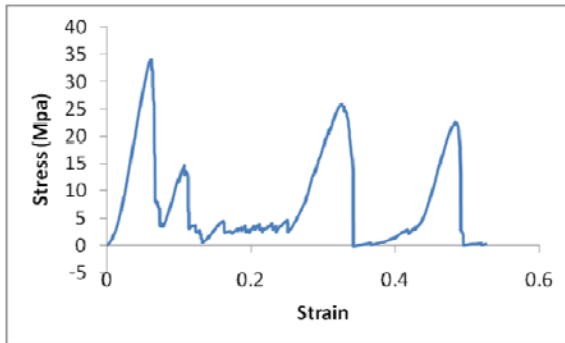
a. Ti6Al4V

b. Pure copper

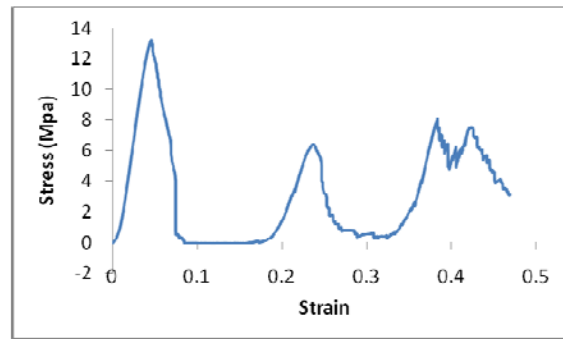
Fig. 5 Compressive tests of the samples

Typical compression strain-stress curves for Ti6Al4V and copper samples are shown in Fig. 6. In comparing the two materials, it is apparent that the Ti6Al4V samples exhibit a failure mode very similar to that of a brittle material. After the initial linear stress-strain region, the stress drops abruptly to a rather low value without apparent yield. During compression testing, the Ti6Al4V samples typically suffered catastrophic failure of one whole layer normal to the loading direction, which corresponded to the steep drop of stress value in the curve. After the first failure, the stress level of the Ti6Al4V samples stays relatively low and stable with increasing strain before entering another linear stress-stress cycle. This corresponds to the loading and subsequent failure of another complete layer.

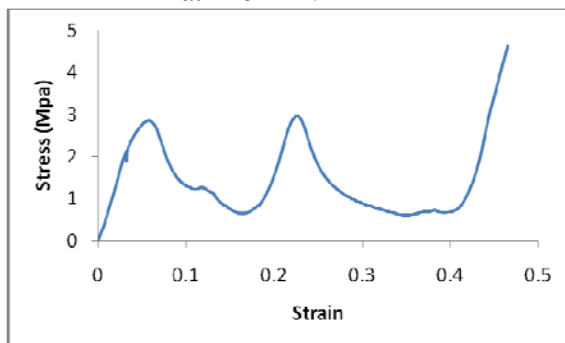
As expected, strain-stress curves for the copper samples showed considerable ductility. After the initial linear stress increase, there exists an apparent yield period. Sample failure is characterized by gradual deformation of the structure without abrupt fracture of individual struts.



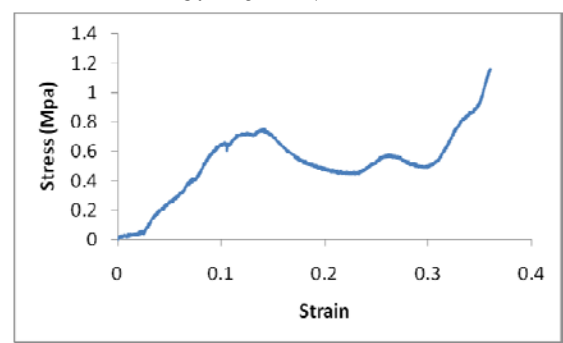
a. Ti6Al4V - D1



b. Ti6Al4V - D2



c. Copper - D1



d. Copper - D2

Fig. 6 Representative stress-strain curves for the compressive samples

The total energy absorbed during the compression was calculated for each sample. The energy absorption by each structure up to 25% strain was obtained by calculating the total areas under the strain-stress curves. This accounts for the total energy absorption of the first layer of the structure. It was expected that ductile materials (e.g. copper) would show a significantly improved energy absorption ability compared to the relatively brittle Ti6Al4V samples. This is reflected by the curves in Fig. 6.

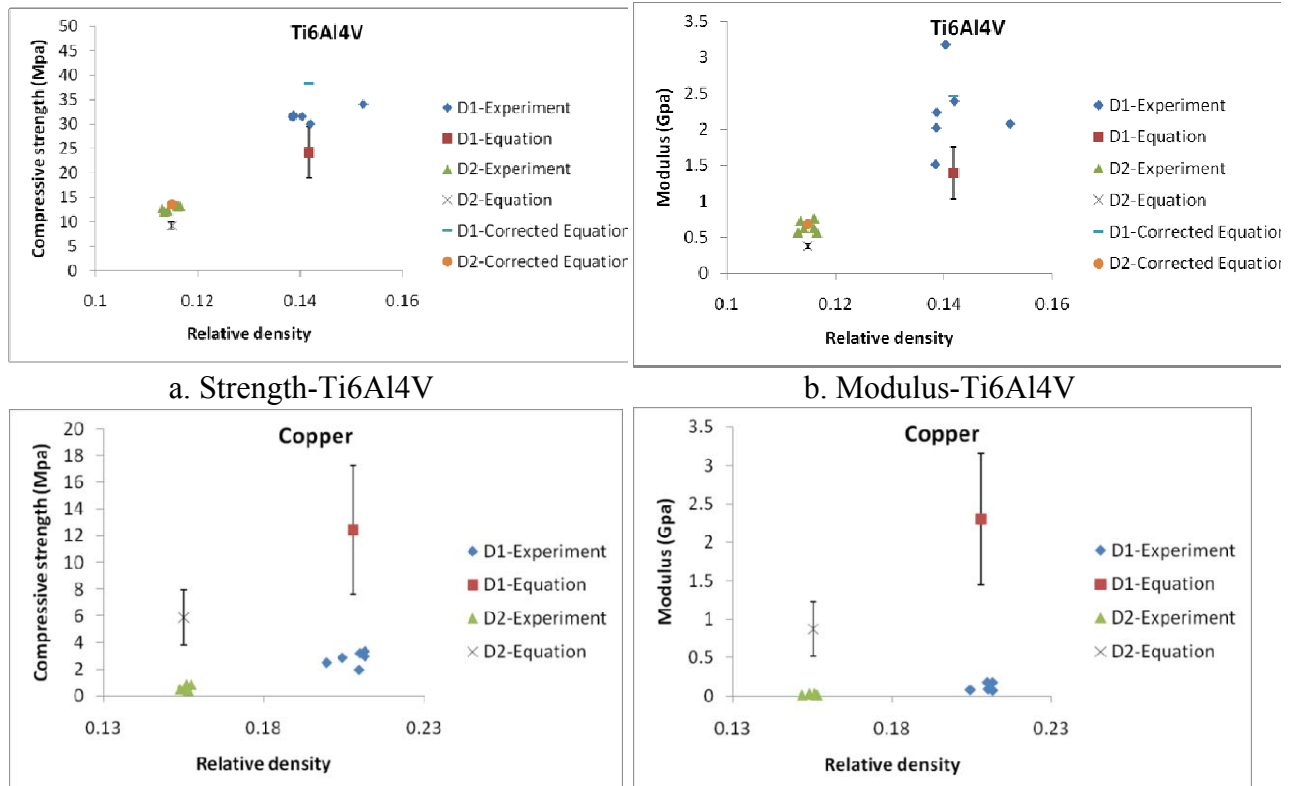
The mechanical properties as well as energy absorption characteristics for the Ti6Al4V and copper samples are shown in Table 3. Significant variation of values was observed for the D2 samples made by copper, which was likely caused by the greater degree of geometrical irregularity at the ends of the struts.

Table 3 Mechanical properties of the samples under compression

Design	Strength (MPa)	Modulus (GPa)	Energy absorption per unit volume (MJ/m ³)	Energy absorption per unit weight (kJ/kg)
Ti6Al4V				
D1	31.765±1.309	2.231±0.567	0.622±0.234	0.984±0.343
D2	12.898±0.508	0.646±0.082	0.432±0.042	0.851±0.092
Copper				
D1	2.804±0.513	0.117±0.054	0.188±0.017	0.101±0.011
D2	0.624±0.204	0.021±0.008	0.057±0.010	0.042±0.007

Discussion

Based on the measurement results of the actual samples, the theoretical prediction of the compressive strength as well as the modulus was obtained. Because of the variation of the design parameters, there exists a range for the resulting mechanical properties, which is shown in Fig. 7, along with the comparison between the theoretical prediction and the experiments. It could be seen that the prediction for Ti6Al4V samples is in relatively good agreement with the experimental results, while the prediction for copper samples is significantly higher than the actual values.



c. Strength-Copper

d. Modulus-Copper

Fig. 7 Comparison between the model and the experiment

For Ti6Al4V samples, the theoretical prediction shows the same trend as the actual experimental values, with the deviation between the prediction and the actual values relatively consistent. This deviation could be largely attributed to the reduced effective length of the re-entrant struts. As shown in Fig. 8 the thickness of the struts causes the actual length of the re-entrant struts that is deflectable to be shorter. This effect becomes more significant as the re-entrant angle becomes smaller. It is difficult to determine the effective length accurately. For the current work, however, it could be roughly estimated that the reduction of the length was between 0.7-0.9mm based on the design configuration. After the correction was applied, the theoretical predictions show considerable improvement of match with the actual values, as also shown in Fig. 7 (a)-(b).

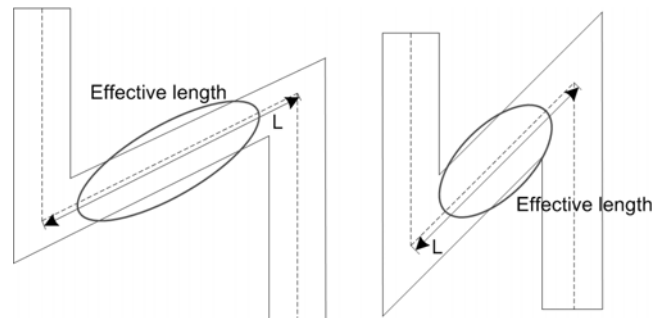


Fig. 8 Demonstration of the reduced effective length for re-entrant struts

For the copper samples, the large difference between the theoretical prediction and the actual results is believed to be largely attributed to large deviations in strut dimensions. From the measurements shown in Table 2, the copper strut dimensions vary by more than 13%. From Eq. (3) and Eq. (4), the strut dimension (t) has a significant effect on the mechanical properties. Fluctuations in strut dimensions will therefore result in large variations in mechanical properties as shown in the error bars in Fig. 7 (c)-(d). In addition, significant layering effect could be observed for the copper parts, as shown in Fig. 9. This indicates potentially weak inter-layer metallurgical bonding. Also visible in Fig. 9 is a large void defect which is marked by the arrow. From the strain-stress curves of some copper samples, it could be reasonably concluded that the yield of some of the struts occurs even at the very early stages of compression, resulting in the curving of the strain-stress curve. With this explanation, it could be estimated that the actual effective strut dimensions for D1 and D2 copper samples are around 0.5-0.7mm. The manufacturing defects could in turn be explained by the large coefficient of thermal conductivity of copper. Due to the severe dissipation of thermal energy during the melting process, it is more difficult to control both the metallurgical integrity and the dimensional accuracy. In the case of current study, both were compromised to a large extent.

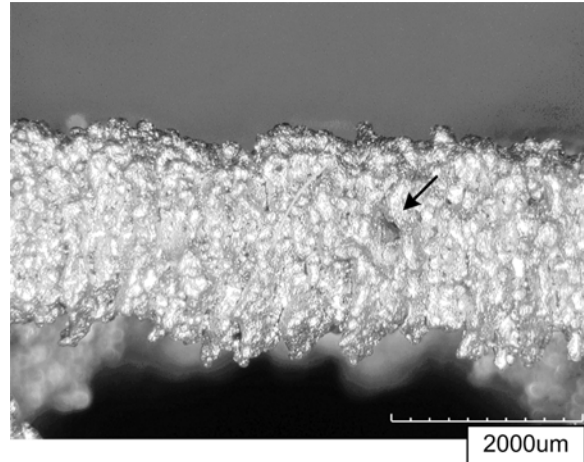


Fig.9 Strut of the copper samples

For most stochastic cellular structures, the strain-stress curve shows an apparent plateau stage after the onset of initial yield [17], which was not observed in all the Ti6Al4V samples, and most of the copper samples. It is known that most of the energy absorption of the cellular structures occurs at the plateau stage, therefore, it could be reasonably expected that the energy absorption ability of the re-entrant lattice samples made by Ti6Al4V was significantly limited. In comparison, copper has much higher ductility, and its strain-stress curve also shows much smoother pattern. Comparing the energy absorption of the Ti6Al4V samples shown in Table 3, design configuration D2 exhibits much lower strength and modulus while absorbing comparable energy per unit weight compared with D1. It is preferred for the structure to exhibit lower peak resistance force in many energy absorption applications, therefore, in the applications where the total weight is limited, designs with greater auxetic behavior (e.g. D2) will be favored.

After the failure of two layers, the copper samples started to densify, which could be characterized by the steady and mostly linear increase of the stress at the end of the strain-stress curves shown in Fig. 6 (c)-(d). Due to the copper's greater ductility, individual struts did not always fracture and detach from the structure. They therefore act as resisting sites for further deformation and facilitate the onset of densification. Fig. 10 shows one of the D2 copper samples after compression. It could be seen that the struts have formed a stable frame structure that behaves more like a densified solid that it would had the struts fractured cleanly from one another.

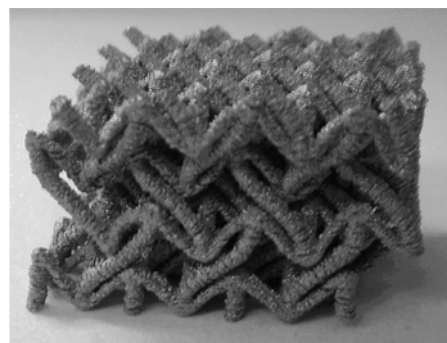


Fig. 10 Compressed copper sample

Conclusion

In this work, a 3D model for a re-entrant lattice structure was presented in which the lattice geometry was defined as a function of four parameters. Two different design configurations were created for comparison in compressive tests using relatively brittle Ti6Al4V and ductile pure copper. Samples were manufactured via the EBM process and evaluated through physical tests. The results were compared with the theoretical predictions, and corrections of the theory were made to compensate for deviations introduced by the manufacturing process.

The results for the Ti6Al4V samples are in reasonably good agreement with the analytical models. On the other hand, the results for the copper samples show consistently large deviation from the predictions, which could be largely attributed to the small effective strut size caused by manufacturing variations such as voids and the step effect. The large thermal conductivity of the copper results in significant sintering effect which contributes to the diminished surface quality of copper parts in the EBM process. More process optimization is therefore needed with this material to improve surface quality and accuracy.

With greater auxetic behavior, the energy absorption per unit weight increases while the maximum react strength (e.g. resistant force) could be controlled in a low level. This makes the structures with large auxetic behavior favorable in the energy absorption applications where weight is a limiting criteria.

References

- [1] Roderic Lakes. Foam Structures with a Negative Poisson's Ratio. *Science*. 235(1987): 1038-1040.
- [2] F. Scarpa, P. J. Tomlin. On the transverse shear modulus of negative Poisson's ratio lattice structures. *Fatigue & Fracture of Engineering Materials & Structures*. Vol 23, 2000, p 717-720.
- [3] F. Scarpa, G. Tomlinson. Theoretical characteristics of the vibration of sandwich plates with in-plane negative Poisson's ratio values. *Journal of Sound and Vibration*. Vol 230, 2000, p 45-67.
- [4] R. S. Lakes, K. Elms. Indentability of Conventional and Negative Poisson's Ratio Foams. *Journal of Composite Materials*. Vol 27, 1993, p 1193-1202.
- [5] K. L. Alderson, V. R. Simkins, V. L. Coenen, et al. How to make auxetic fibre reinforced composites. *Physica Status Solidi (b)*. Vol 57, 2009, p 1865-1874.
- [6] R. S. Lakes. Design Considerations for Materials with Negative Poisson's Ratios. *Journal of Mechanical Design*. Vol 115, 1993, p 676-700.
- [7] Abderrezak Bezazi, Fabrizio Scarpa. Tensile fatigue of conventional and negative Poisson's ratio open cell PU foams. *International Journal of Fatigue*. Vol 31, 2009, p 488-494.
- [8] Abderrezak Bezazi, Fabrizio Scarpa. Mechanical behaviour of conventional and negative Poisson's ratio thermoplastic polyurethane foams under compressive cyclic loading. *International Journal of Fatigue*. Vol 29, 2007, p 922-930.
- [9] F. Scarpa, P. Pastorino, A. Garelli, et al. Auxetic compliant flexible PU foams: static and dynamic properties. *Physica Status Solidi (b)*. Vol 242, 2005, p 681-684.
- [10] F. Scarpa, L. G. Ciffo, J. R. Yates. Dynamic properties of high structural integrity auxetic open cell foam. *Smart Materials and Structures*. Vol 13, 2004, p 49-56.

- [11] F. Scarpa, J. R. Yates, L. G. Ciffo, et al. Dynamic crushing of auxetic open-cell polyurethane foam. *Proceedings of the Institution of Mechanical Engineerings, Part C*. Vol 216, 2002, p 1153-1157.
- [12] Barbara Howell, Pat Prendergast, Larry Hansen. Examination of Acoustic Behavior of Negative Poisson's Ratio Materials. *Applied Acoustics*. Vol 43, 1996, p 141-148.
- [13] F. Scarpa, F. C. Smith. Passive and MR Fluid-coated Auxetic PU Foam - Mechanical, Acoustic, and Electromagnetic Properties. *Journal of Intelligent Material Systems and Structures*. Vol 15, 2004, p 971-979.
- [14] F. Scarpa, W. A. Bullough, P. Lumley. Trends in acoustic properties of iron particles seeded auxetic polyurethane foam. *Proceedings of the Institution of Mechanical Engineers. Part C: Journal of Mechanical Engineering Science*. Vol 218, 2004, p 241-244.
- [15] E. A. Friis, R. S. Lakes, J. B. Park. Negative Poisson's ratio polymeric and metallic foams. *Journal of Materials Science*. Vol 23, 1988, p 4406-4414.
- [16] S. Krenk. *Mechanics and Analysis of Beams, Columns and Cables, 2nd Edition*. Springer, 2001, p 30-31.
- [17] Lorna J. Gibson. *Cellular solids: structure and properties, 2nd edition*. Cambridge University Press, 1997.